JOURNAL OF MATERIALS RESEARCH AND TECHNOLOGY 2022;20:3891–3904

Available online at www.sciencedirect.com

jmr&t Journal of Materials Research and Technology

journal homepage: www.elsevier.com/locate/jmrt

Original Article

Influence of operating parameters on nanobubble-assisted flotation of graphite

Sabereh Nazari [a], *Shaoqi Zhou* [a,b], *Ahmad Hassanzadeh* [c,d], *Jinlong Li* [a], *Yaqun He* [a,**], *Xiangning Bu* [a,b,*], *Przemyslaw B. Kowalczuk* [d]

[a] *School of Chemical Engineering and Technology, China University of Mining and Technology, Xuzhou, 221116, China*

[b] *Key Laboratory of Coal Processing and Efficient Utilization (Ministry of Education), China University of Mining and Technology, Xuzhou, 221116, China*

[c] *Maelgwyn Mineral Services Ltd, Ty Maelgwyn, 1A Gower Road, Cathays, Cardiff, CF24 4PA, UK*

[d] *Department of Geoscience and Petroleum, Faculty of Engineering, Norwegian University of Science and Technology, Trondheim, 7031, Norway*

ARTICLE INFO

Article history:
Received 29 April 2022
Accepted 28 August 2022
Available online 6 September 2022

Keywords:
Nano-bubble-assisted flotation
Graphite
Frother
Operating parameters
Kinetic rate constant

ABSTRACT

Although many studies have focused on processing of lithium-ion batteries (LiBs), there is a considerable lack of information concerning the application of nanobubbles (NBs) in their floatabilities. To cover this knowledge gap, the current study aims at exploring the effect of key operating parameters on flotation of two types of graphite i.e., lithium-ion batteries' graphite (LIBG) and natural ore graphite (NOG) in the presence of NBs. For this purpose, the effects of NB solution ratio, impeller speed, air flow rate, as well as dosage and type of collector and frother on recovery of graphite were investigated in the presence and absence of NBs. Three frothers (i.e., methyl isobutyl carbinol (MIBC), terpenic oil, and 2-octanol), and three collectors (i.e., n-dodecane, kerosene and diesel oil) were employed for comparison purposes using an XFG micro-flotation unit. The hydrodynamic cavitation and dynamic light scattering (DLS) methods were utilized to produce and characterize ultrafine bubbles, respectively. The DLS results confirmed the bubble size distribution ranged between 180 and 400 nm. The maximum recovery of graphite particles (ca. 98%) was obtained for the LIBG particles, at an impeller speed of 1000 rpm, air flow rate of 0.4 L/min, using 2-octanol as a frother, and n-dodecane as a collector. Further, the influential order of the frothers was found as 2-octanol > terpenic oil > MIBC. According to the flotation results, the presence of NBs increased the LIBG flotation recovery and its kinetic rate by 15% and 33%, respectively.

** Corresponding author.
* Corresponding author.
E-mail addresses: yqhe@cumt.edu.cn (Y. He), xiangning.bu@foxmail.com (X. Bu).

https://doi.org/10.1016/j.jmrt.2022.08.137

1. Introduction

Over the last decades, many efforts have been devoted to improve the flotation performance of difficult-to-float ultrafine and coarse particles [1–5]. Exploring possible solutions to mitigate losing valuable minerals in tailings, studying mining options for low-grade ores, and exploring perspectives to reclaim valuable components from accumulated wastes are vital in addressing the challenges [6–8]. The use of nanobubbles (NBs, nanoscopic gaseous cavities not larger than 1 μm) in flotation of ultrafine, fine and coarse particles has been one of the promising solutions to overcome the challenges in their flotation. Thus, in the last decade many scientists have focused on characterization and application of ultrafine bubbles due to their unique physical and physicochemical properties [9–15]. Different methods for generating NBs such as hydrodynamic cavitation [8,16,17], ultrasonic cavitation [18,19], solvent exchange [20,21], temperature raise [22] and electrolysis [23] have been applied. These methods have wide application prospects in flotation due to their simplicity and efficiency [24–27].

Although fundamentals of NBs have not yet been understood thoroughly, great efforts have been made to improve the flotation recovery and kinetics as well as to reduce chemical reagent consumptions. One of the principle arguments is related to the stability of bulk and surface nano-bubbles. Although many studies investigated the properties of bulk nano-bubbles but their stability in aquiouse solutios is still unclear and under discussion in the literature [28,29]. However, the stability of surface nano-bubbles in the presence of hydrophobic particles have been well documented [30,31]. It was found that the application of NBs along with conventional bubbles (CBs) ensures a significant increase in the flotation efficiency of fine, ultrafine, and coarse particles [17,32–37]. NBs have been applied in flotation of various materials (Fig. 1), mainly coal, quartz and for wastewater treatment purposes. Hydrodynamic cavitation-assisted flotation methods have been found more effective than the conventional flotation resulting in elevating recovery and kinetics [37–41].

The literature on the application of NBs in flotation of graphite is still limited. In one of the studies, two flake graphite and one microcrystalline graphite ores were used to investigate the flotation performance in the absence and presence of NBs. Bu, Zhang [42] concluded that the column flotation was more efficient for cleaning the microcrystalline graphite ore in the presence of NBs generated by the hydrodynamic cavitation. The froth layer using column cells was found relatively thicker in comparison with mechanical flotation cells (without NBs). Further, Ma, Tao [43] applied a similar flotation column to upgrade a flake graphite ore. Following this, Li, Xing [39] reported that the graphite flotation performance was not improved by ultrasound pretreatment. The explanation for the NB-assisted flotation using the acoustic cavitation is limited because there is no generally accepted theory of the generation and stability mechanisms of NBs in acoustic fields [29]. Thus, there are no systematic studies on the effect of the type and dose of frothers and collectors as well as operating parameters (i.e., impeller speed and airflow rate) on NB-assisted flotation of graphite.

On other hand, many attempts have been made to improve the flotation performance of lithium-ion batteries' graphite (LIBG) that are always addressed as a major technical challenge. For instance, Zhang, He [44] proposed a selective

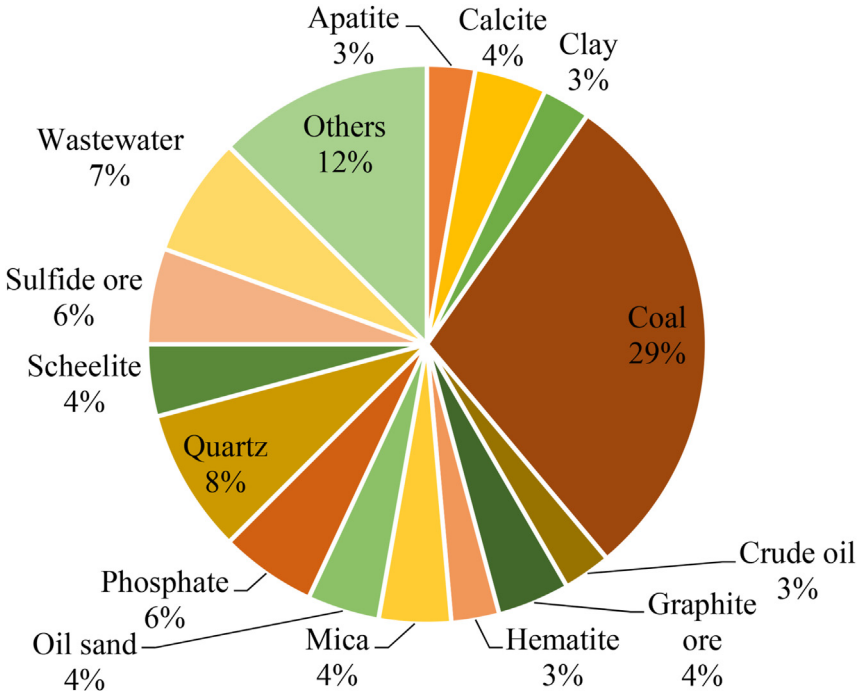

Fig. 1 – Application of NB-assisted flotation. Others refer to the sum count of minerals that only appeared once in the literature. The original data (total of 72 research papers in the attachment: Appendix 1) were collected from the Scopus database (2009–2022).

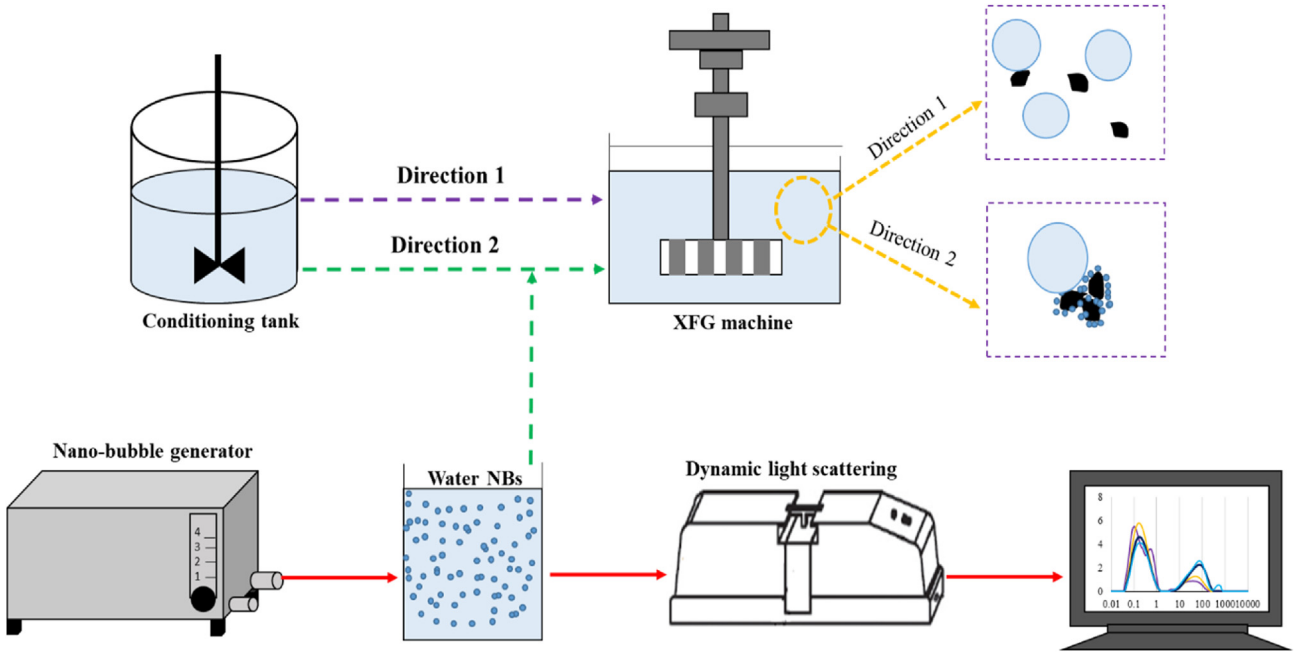

Fig. 2 – A schematic overview of flotation experiments of graphite without (direction 1) and with (direction 2) NBs.

crushing-assisted pyrolysis flotation method for separating and recovering graphite from lithium-ion batteries (LIBs). They showed that the grade and recovery of graphite reached ca. 91% and ca. 81%, respectively. He et al. [45] studied the flotation performance of graphite and valuable electrode materials from the spent LIBs indicating that the recovery of materials was enhanced using the Fenton reagent (a solution of hydrogen peroxide with ferrous iron, typically iron(II) sulfate). Liu et al. [46] proposed a novel method of cryogenic grinding and froth flotation to recover $LiCoO_2$ and graphite from spent LIBs. They concluded that the grade and the recovery rate of materials increased after 9 min of cryogenic grinding. Vanderbruggen et al. [47] studied the flotation behavior of lithium metal oxides and spheroidized graphite from spent LIBs. They observed that the typically used oil-based collectors interacted with both spheroidized graphite and lithium metal oxides, increasing their hydrophobicity and promoting agglomeration. Cheng, Marchetti [48] summarized various modified flotation techniques used for recovering graphite from spent LIBs, like "surface modification + flotation", "grinding + flotation", "thermal treatment + flotation", and "pyrolysis + flotation". It is also expected that NB-assisted flotation can be a promising approach to enhance the flotation performance of graphite from the spent LIBs. Thus, evaluating possible solutions to reduce valuable mineral losses in spent LIBs is vital.

To fill out these knowledge and technological gaps, the influence of NBs on the flotation performance of lithium-ion batteries' graphite (LIBG) and natural ore graphite (NOG) is investigated. Besides that, the impact of several key influential parameters, including the impeller speed, airflow rate, as well as type and concentration (dose) of collectors and frothers, are studied in detail in the presence and absence of NBs. In particular, the flotation kinetics of LIBG and NOG in the absence and presence of NBs are compared. We believe that the findings of this work will help to improve LIBG particle flotation. This research may significantly promote the practical application of NBs in the field of spent LIBs to meet the needs of both environmental protection and sustainable development of energy resources.

2. Materials and methods

2.1. *Materials and reagents*

Two pure graphite samples, lithium-ion batteries' graphite (LIBG) and natural ore graphite (NOG) were purchased from Shenzhen BTR New Energy Material Tech Co., Ltd (Guangdong Province, China) and Tianjin Dengke Chemical Reagent Co., Ltd (Tianjin, China), respectively. Methyl isobutyl carbinol (MIBC, $C_6H_{14}O$, 100.16 g/mol), terpenic oil ($C_{10}H_{18}O_2$, 154.25 g/mol), and 2-octanol ($C_8H_{18}O$, 130.23 g/mol) with the purity of 98% were used as frothers. N-dodecane ($C_{12}H_{26}$, 170.33 g/mol), kerosene ($C_{15}H_{32}$, 321.49 g/mol), and diesel oil (a mix of saturated hydrocarbons and aromatic hydrocarbons, 60–150 g/mol) with the purity of 99% were applied as collectors. These frothers and collectors were used for flotation of graphite particles in the previous studies [46,49,50]. All reagents consumed in the experiments were purchased from Shanghai Aladdin Biochemical Technology Co., Ltd. In all experimental works, the deionized water was used, which temperature, conductivity, and pH were daily monitored. Its pH was kept constant at 7 (natural pH) and a measured conductivity of about 18.2 MΩ cm was reported while generating NBs and carrying out the flotation experiments. These measurements were performed to ensure water purity and consistency throughout the entire experimental work.

Table 1 – Description of applied flotation kinetic models [31].

No.	Model	Formula
1	Classical first-order model	$R = R_{\infty,1}(1 - e^{-K_1 t})$
2	First-order with a rectangular distribution	$R = R_{\infty,2}\left[1 - \frac{1 - e^{-K_2 t}}{K_2\, t}\right]$
3	Fully mixed factor model	$R = R_{\infty,3}\left[1 - \frac{1}{(1 + t/K_3)}\right]$
4	Improved gas/solid adsorption model	$R = \frac{R_{\infty,4} K_4 t}{1 + K_4 t}$
5	Second-order model	$R = \frac{R_{\infty,5}^2 K_5 t}{1 + R_{\infty,5} K_5 t}$
6	Second-order with a rectangular distribution	$R = R_{\infty,6}\left\{1 - \left[\frac{1}{K_6 t}\ln(1 + K_6 t)\right]\right\}$

2.2. Characterization techniques

The particle size distribution (PSD) of samples was measured by a laser particle size analyzer (GSL-1000, Liaoning Instrument Research Institute Co., Ltd, China). Four consecutive measurements were undertaken, from which an average value was calculated. Samples were characterized using an X-ray fluorescence spectrometer (XRF, Bruker S8 Tiger, Germany), and the carbon content (C) in graphite was determined. The crystallographic analysis was carried out with an X-ray diffractometer device (XRD, Bruker D8 Advance, Germany) under Cu Kα radiation using some key parameters, including 35 keV of accelerating voltage, 30 mA of current, 3–75° of scanning range, 0.5 s/step of scan speed. A scanning electron microscope (FESEM, TESCAN MAIA3, Czech Republic) was used to analyze the surface topography of both graphite samples. Fourier transform infrared spectroscopy was conducted using a KBr disk technique and a Fourier transform infrared (FTIR) spectrometer (Germany, Bruker, Vertex80V) in the range of 400–4000 cm^{-1}. Also, the size of NBs was obtained according to the Brownian motion when the dynamic light passed through the quartz cell.

2.3. Generation of NBs

A nanobubble generator developed by the Xia Zhichun Environmental Protection Technology Co., Ltd (Kunming, Yunnan Province, China) was employed to produce NBs through the hydrodynamic cavitation approach (Fig. 2). During the preparation of NBs, an inlet and outlet pipe were included within the generator. After the water was pumped into the inlet pipe, it flowed out of the outlet, then, the power was turned on. Under the action of hydrodynamic cavitation, the gas and liquid were fully mixed to form a milky white gas–liquid mixture rich in NBs. Also, NBs were generated using deionized water without any reagents. The bubble size distribution was evaluated by a dynamic light scattering (DLS) device (Omni, Brookhaven, USA). This equipment was typically used in colloidal suspensions and emulsions for the detection of bubbles in the sub-micron region (lower than 1 μm) [9]. Detailed information regarding the measuring diameter and distribution of NBs using various techniques is given elsewhere [9].

2.4. Flotation experiments

The micro-flotation experiments were carried out using an XFG flotation machine (Nanchang Jianfeng Mining Machinery Manufacturing Co., Ltd.). Two grams of samples were used for each flotation test. First, the influence of NB-containing solution ratio (17, 33, 50, and 67%) was investigated on the flotation recovery using MIBC as one of the well-known frothers. Then, the impeller speed was set at 1000, 1200, 1500, and 1900 rpm for the airflow rates of 0.2, 0.4, and 0.8 L/min, and flotation experiments were conducted with and without NBs. Additionally, the type and concentration (dosage) of collector and frother on the graphite flotation performance were also explored. The pH of the slurry was 7 during conditioning based on the previous work [51] and all experiments were performed at a room temperature of 25 °C.

The slurry containing solid particles and water was conditioned for 1 min after addition of the required amount of collector. The flotation experiments were conducted in two different ways, a certain volume of prepared frother and NBs were added to the flotation cell with 30 s conditioning time as follows (Fig. 2): (I) without NBs, the frother solution was directly added to the flotation cell; (II) with NBs, the frother and NBs were added to the flotation cell at the same time.

The flotation experiments started 30 s after the addition of frother when the air was introduced into the flotation cell. The floating particles were collected over time intervals of 10, 15, 30, and 60 s. All flotation products were collected and dried in a dryer (at 100 °C for 120 min) to determine their weights, and thus mass recoveries and kinetics. All flotation experiments were repeated three times and the average values were presented as the ultimate results.

Flotation kinetic parameters, the ultimate recovery (R_∞, %) and flotation rate constant (k, min^{-1}) are excellent tools to evaluate batch flotation tests under different conditions [52,53]. Numerous mathematical flotation models have been proposed to describe flotation time–recovery profiles [54–56]. In this study, six flotation kinetic models (Table 1) were compared to find the optimal model for the experimental data. The kinetic parameters were calculated using the nonlinear regression and the least-squares method in MATLAB. The fitting performance of different kinetic models was

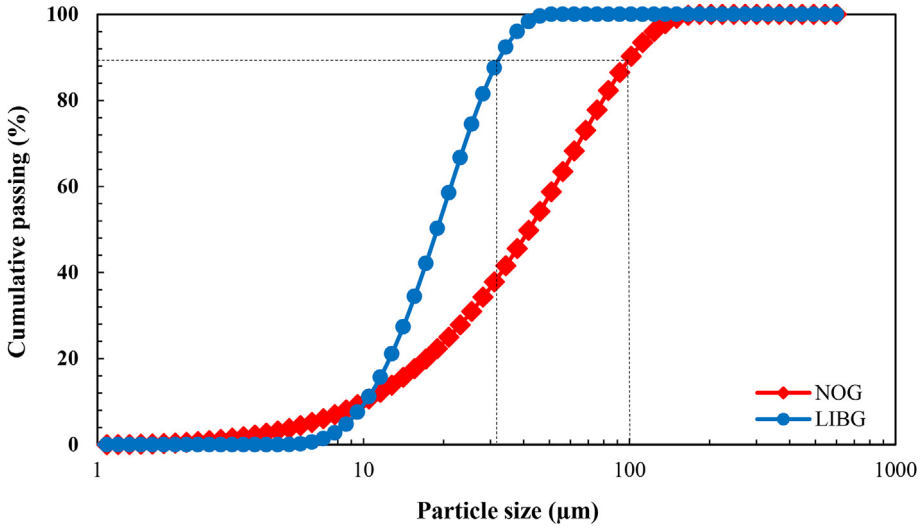

Fig. 3 – Particle size distribution of studied LIBG and NOG samples.

evaluated using two statistical criteria, "R^2 - coefficient of determination and RMSE – root mean square error" [53].

3. Results and discussions

3.1. *Properties of graphite samples*

Fig. 3 shows the particle size distribution of both samples studied in this work. As evidently seen in the PSD graphs, the LIBG and NOG indicate d_{90} of 36 μm, and 101 μm, respectively. It is worth mentioning that the particle size difference of these two samples should be taken into consideration in one-to-one comparisons. Certainly, sufficiently coarse particles can lead to favorable recoveries compared to the fine ones due to the efficient sub-processes in particle-bubble interactions. Detailed information in this regard can be found elsewhere exemplifying the impact of particle density for the chalcopyrite and galena [57] and chalcopyrite and quartz [58]. This can create a significant change in case of dense particles, while for light ones, like graphite, this difference can be relatively lower but absolutely not negligible.

As seen in Table 2, the content of C in both samples is very high (99.8 and 99.7 wt.%, respectively for the LIBG and NOG) demonstrating their high purities. Other impurities such as Ru, Mo, S, Zr, Fe, Cu, and Si were less than 0.081 wt.%.

XRD patterns of samples using two types of surfactants were shown in Fig. 4. The patterns revealed that graphite is the dominant component of the samples. Results reveals that main diffraction peaks appear at 26° and 54°.

Fig. 5 shows the microstructure of the samples which manifests the spherical shape with scaly flakes. The sphericity is an important factor in anode density, because the higher the graphite density, the more energy density exists at the level of full cell. The spherodized shape was conserved during the recycling process, which is an important requirement for anode production [59].

FTIR spectra of two samples obtained are shown in Fig. 6. The stronger broadening band from 998.62 to 1110.69 cm^{-1} for CH was assigned to the in-plane bending vibration of the aromatic ring. The skeleton vibration bonds at 1444.29, 1493.81, and 1574.60 cm^{-1} can be assigned to the aromatic ring. The band at the 1066.39 cm^{-1} was related to the aromatic ester C–O–C systematic stretching. Stretching bonds at 2903.78 and 2997.60 cm^{-1} can be corresponded to the CH_3 antisymmetric and symmetric stretching [60].

3.2. *NB size distributions*

The NBs generator was operated under different conditions (airflow rate 0, 0.5, 1, 1.5, and 2 L/min, and preparation time 1, 2, 4, 6, 8, and 10 min). It was found that when the generation time and airflow rate exceeded, the bubble size increased. Therefore, to ensure the generation of NBs, the airflow rate of 0.5 L/min, and preparation time of 2 min were selected for the flotation experiments. Fig. 7 illustrates the distribution of NBs determined by the DLS technique. The results showed that bubble size distribution ranges between 180 and 400 nm, with the mean diameter of 300 nm.

3.3. *Effect of NB-containing solution ratio*

The flotation results of LIBG and NOG particles with different ratios of NB-containing water solutions are illustrated in Fig. 8.

Table 2 – XRF analysis of studied LIBG and NOG samples.

Composition	C	Ru	Mo	S	Zr	Fe	Cu	Si
LIBG (wt. %)	99.8	0.066	0.044	0.030	0.022	0.021	0.01	0.007
NOG (wt. %)	99.7	0.081	0.064	0.051	0.041	0.031	0.021	0.011

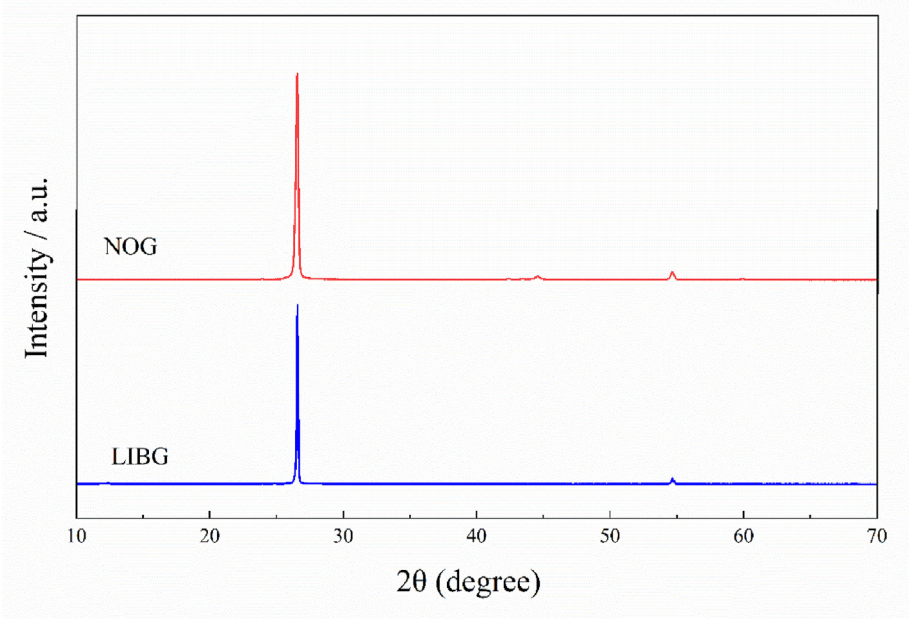

Fig. 4 – XRD patterns for LIBG and NOG samples.

One can see that the LIBG flotation performance is significantly favourable than that of NOG in the absence and presence of NBs with MIBC as a frother. Conditions for the flotation experiments were determined by preliminary tests. As seen, by exceeding the amount of water solution containing NBs the mass recovery linearly increases. This is due to the boost in the number (i.e., concentration) of NBs in the pulp as the proportion of NBs rises. With the heightened concentration of NBs, the probability of their collision and adhesion to the hydrophobic surface of particles improves. This mechanism was presented in detail elsewhere [8,32] for both fine chalcopyrite and coarse quartz particles. Since 67% NB-containing solution ratio provided the best results, it was applied for the rest of flotation experiments.

It is interesting to note that LIBG particles ($d_{90} = 36$ μm) has a greater average size than that of NOG particles ($d_{90} = 101$ μm). The coarser particles have a greater collision probabilities with bubbles, which leads to a superior flotation recovery and flotation rate constant [61,62]. It is expected that LIBG particles have a poorer flotation recovery compared to the NOG particles mostly because of their finer particle sizes. However, it is observed from Fig. 8 that LIBG particles obtained a greater flotation recovery than that of NOG particles. One reason can be attributed to the surface properties of the LIBG

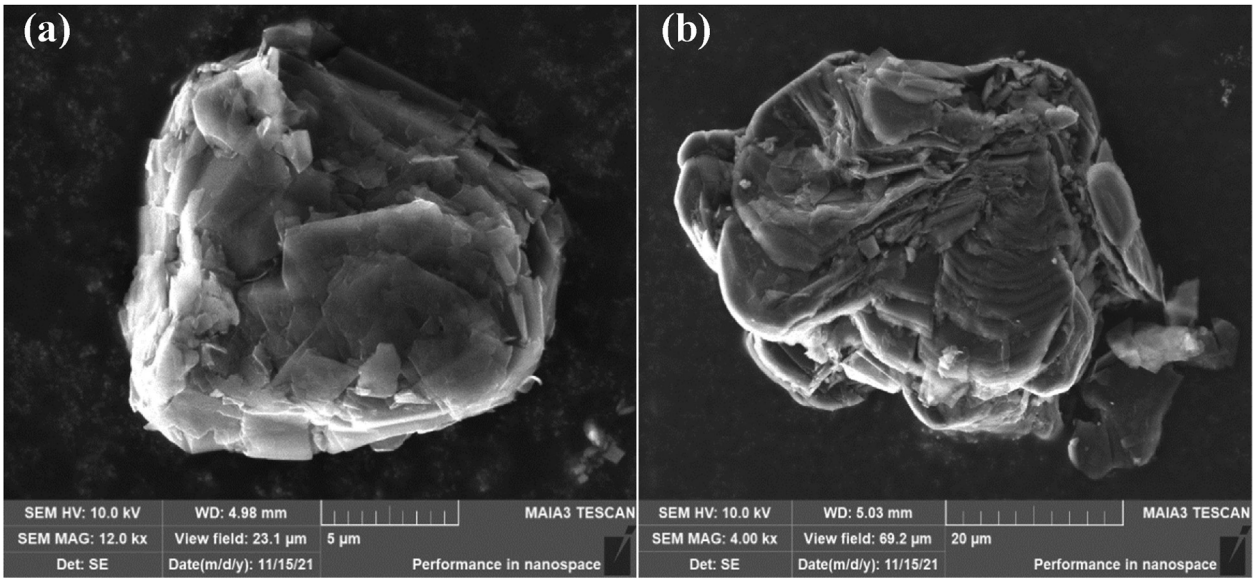

Fig. 5 – SEM pictures of (a) LIBG and (b) NOG graphite particles.

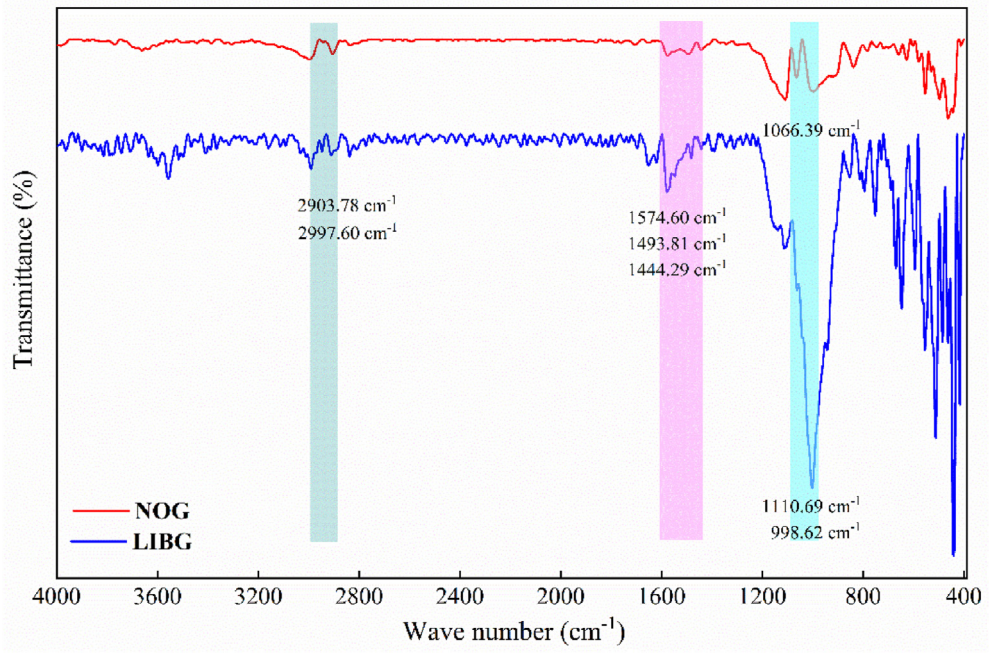

Fig. 6 – FTIR analysis of the samples.

particles which were covered by phenolic resin that significantly promotes the hydrohobicity of LIBG particles [63].

3.4. *Effect of impeller speed and air flow rate*

Impeller speed and airflow rate have an important role in flotation of fine and coarse particles. They are directly related to many sub-processes such as suspension of particles in the pulp, dispersion of air into bubbles, as well as probability of bubble-particle collision, attachment, and detachment. Turbulence leads to disruption of bubble-particle aggregates in a flotation cell. This means that the turbulence should be enough in order not to disturb bubble-particle aggregates [64,65]. However, their impact on the graphite flotation in the presence of NBs is not well explored, which is covered in this section.

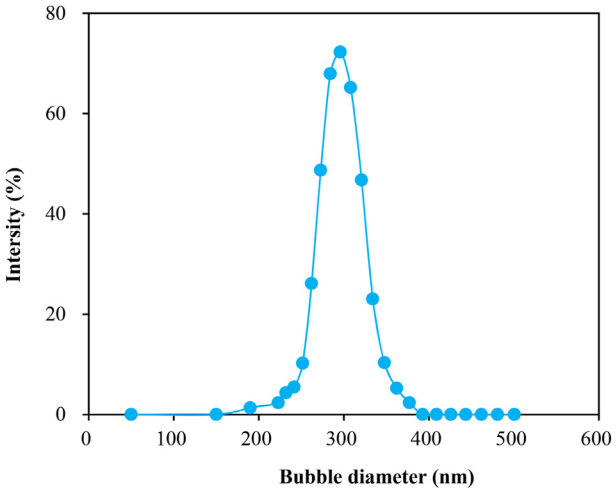

Fig. 7 – Nano-bubble size distribution.

Recovery of flotation at different impeller speeds and airflow rates is shown in Figs. 9 and 10 in the presence and absence of NBs. It can be seen that irrespective of the presence/absence of NBs and type of graphite particles (i.e., LIBG, and NOG), the flotation recovery enhanced with the increase in the airflow rate and hydrodynamics (i.e., impeller speed). With enhancing the air flow rate from 0.2 to 0.8 L/h the amount of dissolved gas in the solution increased and led to increase the flotation recovery. However, it should be noted that the excessive airflow rate of 0.8 L/min caused the mechanical entrainment in this type of flotation device. Also, for a given impeller speed, the amount of air in a cell might increase. When more air is forced through the impeller, its residence time in the shear zone decreases. Although the concentration of air in the cell increases, this air is in the form of larger bubbles and the value of the rate constant remains almost unaffected [66,67].

Our results showed that the presence of NBs increased the flotation performance of the particles, and the most significant difference was observed for the impeller speed of 1000 rpm and airflow rate 0.4 L/min. Thus, these parameters were chosen for conducting further tests, since it allows to leave a margin in the recovery if other parameters such as NBs effect or collector and frother dosage would significantly reduce or increase the flotation performance. Since the ability of conventional air bubbles to carry particles declines as particle size increases. Accordingly, NBs increased the likelihood of bubble particle collisions and attachments, although some aggregates of bubble particles were detachable from the pulp [7,14,33].

3.5. *Impact of frother type and concentration*

The type and quantity of reagents are one of the most important variables in flotation. The control of reagent

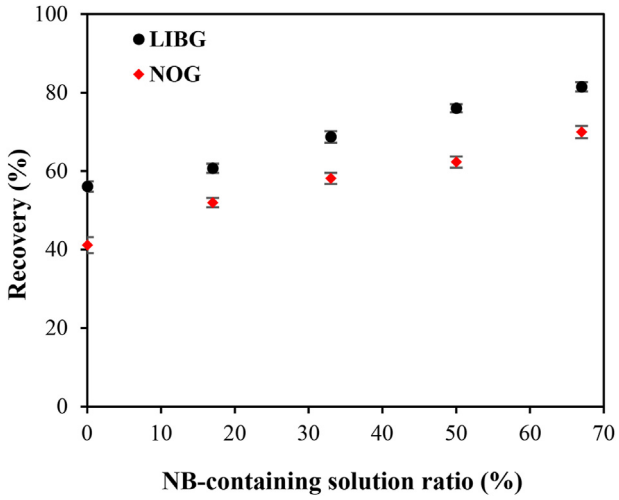

Fig. 8 – Effect of NBs-containing solution ratio on collectorless flotation of graphite (frother MIBC 7 mg/L, impeller speed 1000 rpm, and air flow rate 0.4 L/min).

additions is another important aspect of the flotation strategy. Figs. 11 and 12 show the effect of different types and concentrations of frothers on the collectorless flotation of studied samples without and with NBs.

One can see from Figs. 11 and 12 that there was no flotation of LIBG in the absence of frother, while the recovery of NOG was over 37%. The flotation recovery increases with increasing the frother dosage and then stabilizes, as shown in Figs. 11 and 12.

The highest and lowest recoveries for particles were obtained with 2-octanol and MIBC, respectively. In the case of LIBG, the flotation recovery for 2-octanol plateaued at the frother concentration of 7 and 14 mg/L in the presence and absence of NBs, respectively. However, for terpenic oil and MIBC, the flotation recovery plateaued at the frother concentration of 28 mg/L in the presence of NBs. With respect to the results shown in Fig. 12, the optimum frother dosage for recovering the entire NOG particles without NBs is determined as 14, 28, and 40 mg/L for 2-octanol, terpenic oil, and MIBC, respectively. In the presence of NBs, the optimal dosage of frother was 14 mg/L for all frothers. It is also evident that the presence of NBs caused a strong synergistic effect. The floatability of graphite particles is higher compared to flotation in the absence of NBs. However, the difference in floatability with and without NBs diminishes with a further increase in the frother concentration. Above a certain concentration, the recovery was practically identical or even smaller as observed for flotation of LIBG in the absence of NBs (Fig. 11). This trend was observed for all types of frothers used (i.e. MIBC, terpenic oil, 2-octanol). The mechanism of synergistic effect in the presence of NBs needs further investigation. In the presence of NBs, there was a high tendency for bubbles and particles to attach. NBs covered the surface of mineral particles and played a bridging role among the CBs, which collected the particles more readily and improved the particle-bubble attachment efficiency [11,13]. Finally, the agglomeration and attachment between bubble-particle became easier, which resulted in higher recovery [8,68–71]. Also, NBs reduced the repulsive force between solid particles since the particles became less negatively charged. Moreover, NBs can act as secondary collectors to reduce reagent consumption during flotation [11,13,32]. According to Zhou et al. (2021) [72], the collision angle and mass of particles have a major impact on the bubble-particle attachment. Fine particles moved with the fluid and collide mainly with bubbles in the horizontal direction. They also had a low energy conversion rate, along with a short contact time. Based on their findings, they concluded that the attachment force in the presence of NBs was greater for solid surfaces due to the increase in the hydrophobicity expressed by the contact angle. Also, some researchers suggested a potential mechanism behind the increase in the contact angle caused by NBs. A solid surface with no NBs to cover it exhibits a lower contact angle. When NBs were frosted on a solid surface, attachment of a bubble to the surface was achieved through the coalescence of the conventional bubbles with a few tiny bubbles on the solid surface. A significant increase in the

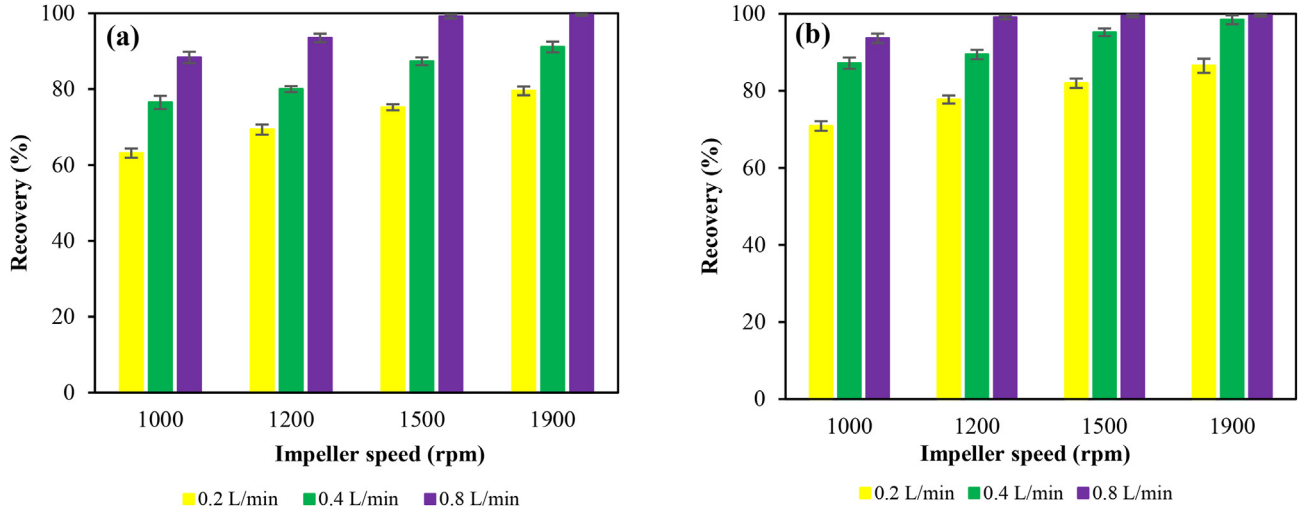

Fig. 9 – Effect of impeller speed and air flow rate on the collectorless flotation of LIBG (a) without and (b) with NBs (2-octanol 3 mg/L, 67% NBs-containing solution ratio).

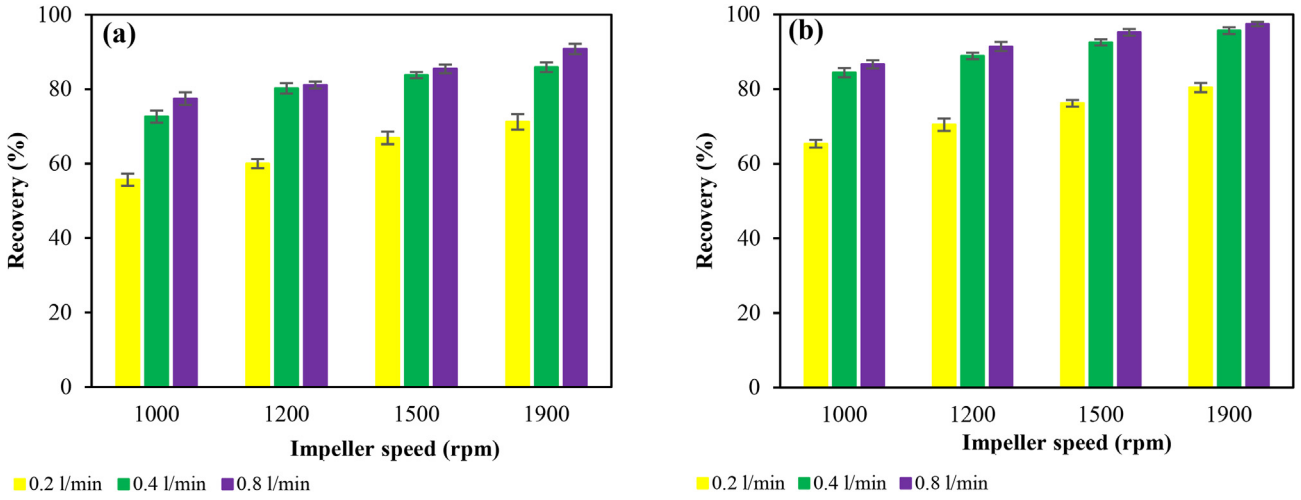

Fig. 10 – Effect of impeller speed and air flow rate on the collectorless flotation of NOG (a) without and (b) with NBs (2-octanol 3 mg/L, 67% NB-containing solution ratio).

contact area was the result of coalescence since the NBs could not easily move from the solid surface [8,73].

3.6. *Impact of collector type and concentration*

Fig. 13 shows the recovery of graphite with different collectors in the presence and absence of NBs. The results showed that the recovery of graphite particles with NBs was approximately 15% higher than that without NBs at the same concentration of collector. The highest recovery was obtained for LIBG particles with dodecane. The influential order of the collectors and frothers was n-dodecane/2-Octanol > kerosene/2-octanol > diesel oil/2-octanol. In this regard, Gontijo et al. [2] illustrated that as the collector increased the particle hydrophobicity, it accelerated particle-bubble attachment and liquid film drainage.

For collectorless flotation, the flotation recovery for LIBG particles is greater than that of NOG particles at the same condition, which is attributed to the presence of hydrophobic coating (phenolic resin) on the LIBG particles. However, it is seen from Fig. 13 that the flotation recovery of NOG particles is very close to that of LIBG particles, which indicates that the presence of a collector can bridge the gap in flotation recovery between LIBG and NOG particles. It is notable that the collector flotation recovery of LIBG particles is greater than that of NOG particles in the presence of NBs. This finding can be due to the nature of LIBG particles having higher hydrophobicity, which is helpful for the adsorption of NBs on the particle surface compared to the NOG particles.

3.7. *Flotation kinetics*

The details of calculation results of six kinetic models under different conditions are given in the supplemental (appendix No. 2). Fig. 14 is the comparison of fitting performance (R^2 and RMSE) of different models. It is observed from Fig. 14 that R^2, and RMSE curves of models 3, 4, and 5 were overlapped completely. This phenomenon is due to that the expressions for models 3, 4, and 5 are same from the mathematical point of view [52,54]. Compared to other models, model 1 (the classic first-order model) has the largest R^2 values and the smallest RMSE values. Meanwhile, the calculated R_∞ values calculated by models 2–6 are larger than 100%. As a comparison, the calculated R_∞ of model 1, values were smaller than 100% (apart from in one special situation). The phenomenon (R_∞>100%) is commonly observed from the kinetic fitting process of coal and graphite having an excessively high flotation recovery [54,61]. Further studies for the flotation

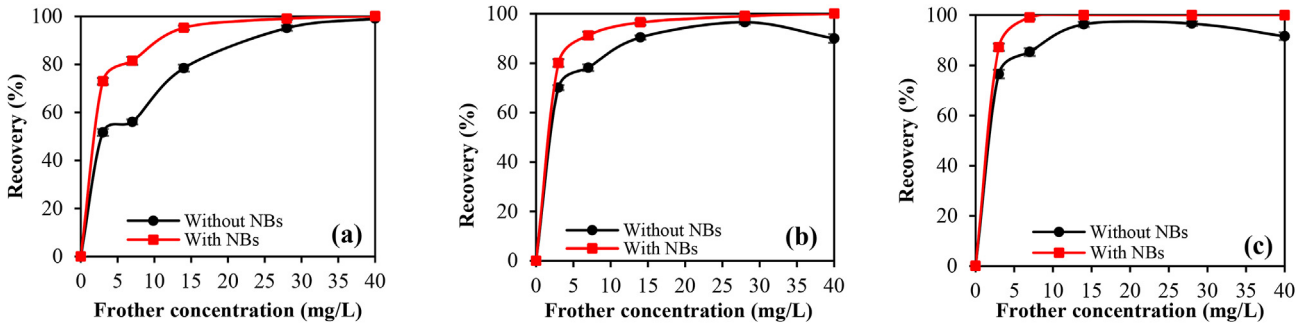

Fig. 11 – Effect of frother concentration and type (a) MIBC, (b) terpinic oil, and (c) 2-octanol on collectorless flotation of LIBG (impeller speed 1000 rpm, and airflow rate 0.4 L/min, 67% NBs-containing solution ratio).

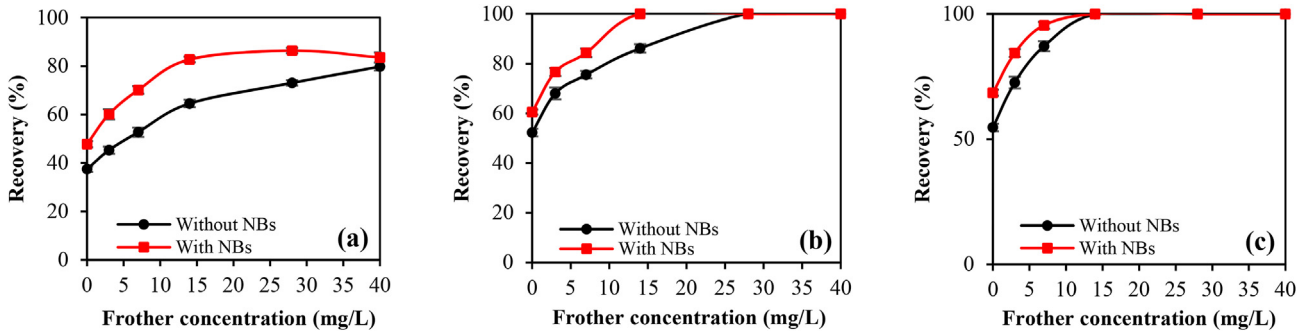

Fig. 12 – Effect of frother concentration and type (a) MIBC, (b) terpinic oil, and (c) 2-octanol on collectorless flotation of NOG (impeller speed 1000 rpm, and airflow rate 0.4 L/min, 67% NBs-containing solution ratio).

kinetics of NBs flotation should be performed to modify the equation of flotation kinetic models from the perspectives of the order of flotation and flotation rate constant distribution function. The classical first-order kinetic model is the most commonly used model to fit the flotation kinetics results [33,35,37,54,55,74–77]. Thus, the classical first-order flotation model was used to evaluate the flotation kinetic results for both LIBG and NOG graphite particles in the presence of NBs. The flotation kinetic results (flotation rate constant, k) for both LIBG and NOG graphite particles at different impeller speeds are given in Fig. 15.

It can be seen that a 33% increase in the flotation rate was achieved with NBs. It is evident from all graphs that the flotation rate constant was significantly higher when NBs were present in the pulp. The unique properties of NBs are naturally capable of enhancing flotation kinetics [7,10,11]. NBs can become stable and remain in the solution for a long time depending on its internal gas pressure, gas composition and solution chemistry of the continuous phase [28,78–81]. The type of gas has a significant effect on the stability of NBs. CO_2 NBs, for instance, have a much shorter lifetime (only 1–2 h) as compared to air bubbles, since CO_2 has a lower atmospheric pressure and is more soluble in water. However, stabilization can also be achieved by causing an influx of gas into the bubble. To maintain a stable dynamic equilibrium, and therefore stable NBs, the influx of gas must be greater than the outflux at small bubble sizes [82,83].

It is considered that the small bubbles have a propensity to spread and their presence at the surface of minerals subsequently facilitates film rupture and attachment of CBs bubbles. Thus, the presence of NBs increases the probability of particle-bubble attachment, decreases the particle-bubble detachment, resulting in an increase in the flotation performance [2,84]. In the presence of NBs, coarse particles attach more easily to CBs. Although NBs do not have sufficient buoyancy to float coarse particles by themselves, the surface of a coarse particle coated with NBs is more hydrophobic than the surface of a particle without NBs [10,11]. It has been demonstrated that NBs can nucleate on ultrafine particles without colliding, and the formation of aggregates can enhance flotation performance [17]. Vaziri Hassas et al. [83] showed that attachment time in the NBs solution is reduced significantly from 30 ms in N_2 saturated solution to less than 10 ms (~5 ms) in CO_2 saturated solution. Enhanced flotation is due to decrease in attachment time. Furthermore, the CO_2 bubbles showed greater elasticity than the N_2 bubbles. CO_2 bubbles' elasticity makes them more likely to attach to particles. According to Albijanic et al. [85], short attachment times indicate strong affinity of particles to

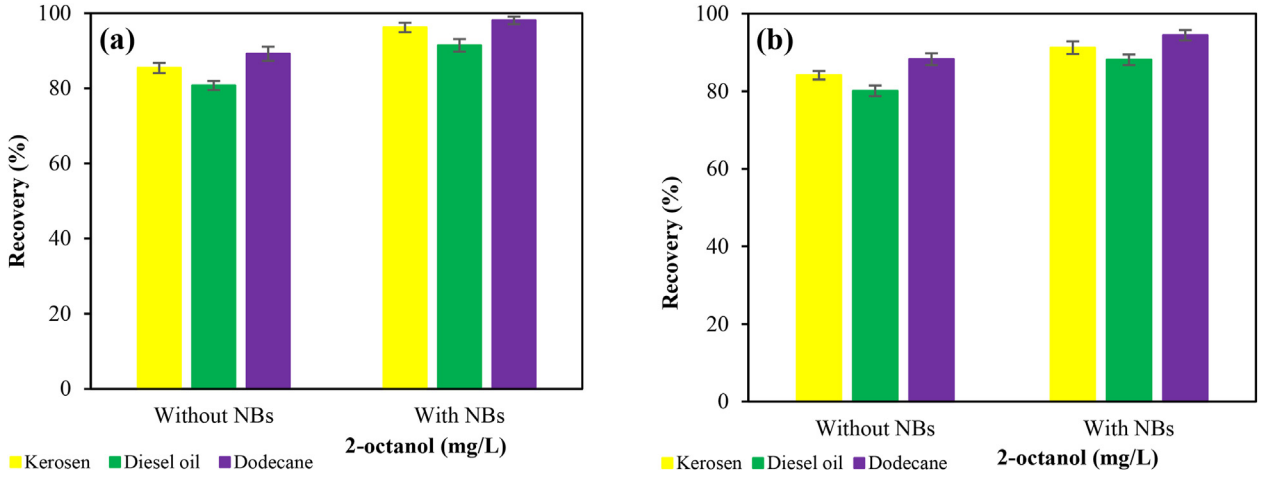

Fig. 13 – Effect of collector type on flotation recovery of (a) LIBG (b) NOG particles (collector dosage: 3 mg/L, frother 2-octanol 3 mg/L, air flow rate 0.4 L/min, impeller speed 1000 rpm, 67% NB-containing solution ratio).

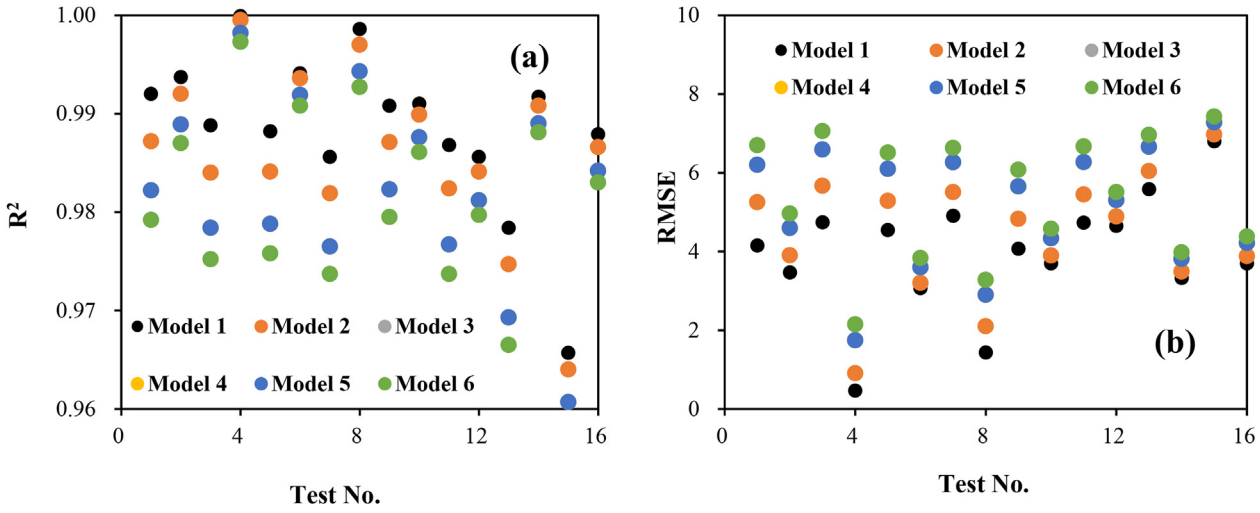

Fig. 14 – Comparison of fitting performance ((a) R^2 and (b) RMSE) of different models.

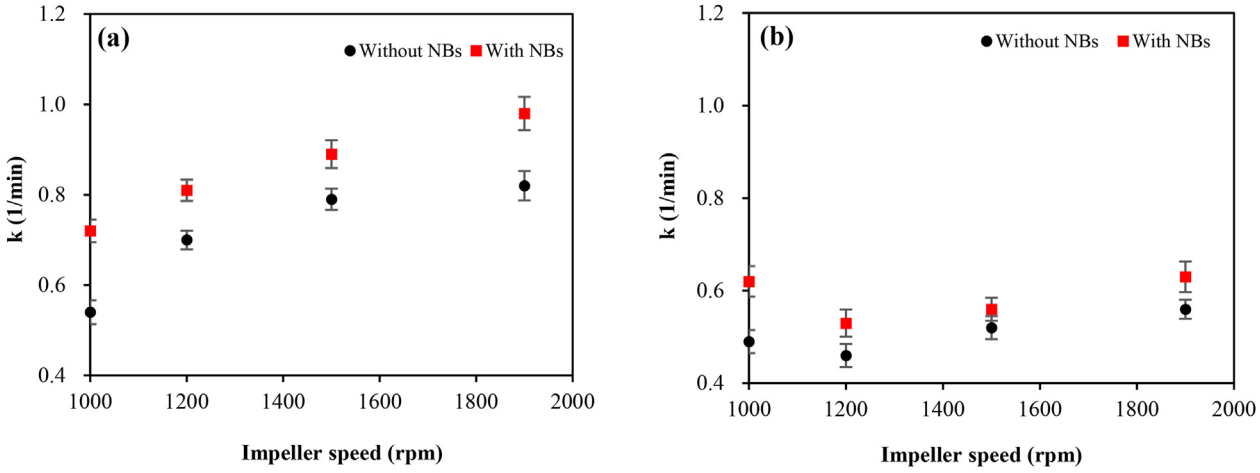

Fig. 15 – Effect of impeller speed and air flow rate on the kinetics of collectorless flotation of (a) LIBG and (b) NOG in the absence and presence of NBs (particles, 2-octanol 3 mg/L, air flow rate 0.4 L/min, 67% NBs-containing solution ratio).

gas phase and higher flotation recovery, whereas long attachment times indicate weak affinity for bubbles and lower flotation recovery.

4. Conclusions and future works

In this study, NBs were produced using a generator based on the hydrodynamic cavitation method. The size of NBs was detected between 180 and 400 nm, with a mean diameter of 300 nm. Followings are some of the key findings highlighted in this work:

- Experimental results indicated that flotation recovery of graphite particles with NBs increased up to 15% depending on the particle size, impeller speed and air flow rate.
- The maximum flotation recovery at the impeller speed of 1000 rpm and airflow rate of 0.4 L/min was obtained with 2-octanol as a frother and n-dodecane as a collector. Using NBs as a secondary collector decreased collector dosage, and a similar reduction was observed in the frother dosage.
- Because of the presence of phenolic resin coating, LIBG particles showed a greater flotation recovery compared to the NOG particles.
- Also, the influential order of the frothers was shown as 2-octanol > Terpenic oil > MIBC, respectively. Furthermore, considering that 2-octanol was steady and of the highest influence, the n-dodecane-2-Octanol combination was the most influential one, followed by kerosene/2-octanol-2 and diesel oil/2-octanol.
- The results of the flotation rate constants showed that the flotation rate constants (k) were always higher with NBs. Flotation rate constant was improved up to 33% by the aggregation of graphite particles caused by the formation of NBs on the surface of hydrophobic particles.

There are no comparative results between nano- and micro-bubbles on the recovery and kinetic of graphite

particles. It is therefore recommended that further research should be conducted in this regard. The effect of NBs and MBs on the recovery, grade, and separation efficiency of spent LIBs can be investigated by considering the result of this research for the graphite particles.

Comprehensive comparison among bulk and surface NBs on the recovery and kinetic of the spent LIBs can be a matter of further investigation.

Author contributions

Sabereh Nazari: conceptualization, investigation, writing-original draft preparation. **Yaqun He**: supervision, conceptualization, methodology, investigation, review and editing, resources. **Ahmad Hassanzadeh**: methodology, investigation, writing -review & editing, visualization. **Shaoqi Zhou**: methodology, software, validation, formal analysis, investigation. **Jinlong Li**: formal analysis, software; review & editing. **Xiangning Bu**: investigation, review & editing. **Przemyslaw Kowalczuk**: investigation, writing-review & editing, visualization. All authors have read and agreed to the published version of the manuscript.

Declaration of Competing Interest

The authors declare that they have no known competing financial interests or personal relationships that could have appeared to influence the work reported in this paper.

Acknowledgments

This work was supported by the Fundamental Research Funds for the Central Universities (2022QN1072).

Appendix A. Supplementary data

Supplementary data related to this article can be found at https://doi.org/10.1016/j.jmrt.2022.08.137.

REFERENCES

[1] Trahar WJ, Warren LJ. The floatability of very fine particles — a review. Int J Miner Process 1976;3(2):103–31.
[2] De F, Gontijo C, Fornasiero D, Ralston J. The limits of fine and coarse particle flotation. Can J Chem Eng 2007;85(5):739–47.
[3] Jameson GJ. Advances in fine and coarse particle flotation. Can Metall Q 2010;49(4):325–30.
[4] Farrokhpay S, Filippov L, Fornasiero D. Flotation of fine particles: a review. Miner Process Extr Metall Rev 2021;42(7):473–83.
[5] Hassanzadeh A, Safari M, Hoang DH, Khoshdast H, Albijanic B, Kowalczuk PB. Technological assessments on recent developments in fine and coarse particle flotation systems. Miner Eng 2022;180:107509.
[6] Rulyov NN, Sadovskiy DY, Rulyova NA, Filippov LO. Column flotation of fine glass beads enhanced by their prior heteroaggregation with microbubbles. Colloids Surf A Physicochem Eng Asp 2021;617:126398.
[7] Nazari S, Hassanzadeh A. The effect of reagent type on generating bulk sub-micron (nano) bubbles and flotation kinetics of coarse-sized quartz particles. Powder Technol 2020;374:160–71.
[8] Ahmadi R, Khodadadi DA, Abdollahy M, Fan M. Nano-microbubble flotation of fine and ultrafine chalcopyrite particles. Int J Min Sci Technol 2014;24(4):559–66.
[9] Nazari S, Hassanzadeh A, He Y, Khoshdast H, Kowalczuk PB. Recent developments in generation, detection and application of nanobubbles in flotation. Minerals 2022;12(4):462.
[10] Fan M, Tao D, Honaker R, Luo Z. Nanobubble generation and its application in froth flotation (part I): nanobubble generation and its effects on properties of microbubble and millimeter scale bubble solutions. Min Sci Technol 2010;20(1):1–19.
[11] Fan M, Tao D, Honaker R, Luo Z. Nanobubble generation and its applications in froth flotation (part II): fundamental study and theoretical analysis. Min Sci Technol 2010;20(2):159–77.
[12] Nazari S, Chelgani SC, Shafaei SZ, Shahbazi B, Matin SS, Gharabaghi M. Flotation of coarse particles by hydrodynamic cavitation generated in the presence of conventional reagents. Separ Purif Technol 2019;220:61–8.
[13] Sobhy A, Tao D. Nanobubble column flotation of fine coal particles and associated fundamentals. Int J Miner Process 2013;124:109–16.
[14] Pourkarimi Z, Rezai B, Noaparast M. Nanobubbles effect on the mechanical flotation of phosphate ore fine particles. Physicochem Probl Mineral Process 2018;54(2):278–92.
[15] Farrokhpay S, Filippova I, Filippov L, Picarra A, Rulyov N, Fornasiero D. Flotation of fine particles in the presence of combined microbubbles and conventional bubbles. Miner Eng 2020;155:106439.
[16] Nazari S, Shafaei SZ, Shahbazi B, Chelgani SC. Study relationships between flotation variables and recovery of coarse particles in the absence and presence of nanobubble. Colloids Surf A Physicochem Eng Asp 2018;559:284–8.
[17] Tao D, Wu Z, Sobhy A. Investigation of nanobubble enhanced reverse anionic flotation of hematite and associated mechanisms. Powder Technol 2021;379:12–25.
[18] Yasuda K, Matsushima H, Asakura Y. Generation and reduction of bulk nanobubbles by ultrasonic irradiation. Chem Eng Sci 2019;195:455–61.
[19] Farmer AD, Collings AF, Jameson GJ. Effect of ultrasound on surface cleaning of silica particles. Int J Miner Process 2000;60(2):101–13.
[20] Xiao Q, Liu Y, Guo Z, Liu Z, Lohse D, Zhang X. Solvent exchange leading to nanobubble nucleation: a molecular dynamics study. Langmuir 2017;33(32):8090–6.
[21] Yang S, Dammer SM, Bremond N, Zandvliet HJW, Kooij ES, Lohse D. Characterization of nanobubbles on hydrophobic surfaces in water. Langmuir ACS J Surf Colloids 2007;23(13):7072–7.
[22] Zhou W, Wu C, Lv H, Zhao B, Liu K, Ou L. Nanobubbles heterogeneous nucleation induced by temperature rise and its influence on minerals flotation. Appl Surf Sci 2020;508:145282.
[23] Yang S, Tsai P, Kooij ES, Prosperetti A, Zandvliet HJ, Lohse D. Electrolytically generated nanobubbles on highly orientated pyrolytic graphite surfaces. Langmuir 2009;25(3):1466–74.
[24] Xiao W, Zhao Y, Yang J, Ren, Yang W, Huang X, et al. Effect of sodium oleate on the adsorption morphology and mechanism of nanobubbles on the mica surface. Langmuir ACS J Surf Colloids 2019;35(28):9239–45.

[25] Zimmerman WB, Tesař V, Bandulasena HCH. Towards energy efficient nanobubble generation with fluidic oscillation. Curr Opin Colloid Interface Sci 2011;16(4):350–6.
[26] Zhou S, Wang X, Bu X, Shao H, Hu Y, Alheshibri M, et al. Effects of emulsified kerosene nanodroplets on the entrainment of gangue materials and selectivity index in aphanitic graphite flotation. Miner Eng 2020;158:106592.
[27] Cho S-H, Kim J-Y, Chun J-H, Kim J-D. Ultrasonic formation of nanobubbles and their zeta-potentials in aqueous electrolyte and surfactant solutions. Colloids Surf A Physicochem Eng Asp 2005;269(1):28–34.
[28] Alheshibri M, Qian J, Jehannin M, Craig VSJ. A history of nanobubbles. Langmuir 2016;32(43):11086–100.
[29] Bu X, Alheshibri M. The effect of ultrasound on bulk and surface nanobubbles: a review of the current status. Ultrason Sonochem 2021;76:105629.
[30] Sun Y, Xie, Peng Y, Xia, Sha J. Stability theories of nanobubbles at solid–liquid interface: a review. Colloids Surf A Physicochem Eng Asp 2016;495:176–86.
[31] Yasui K, Tuziuti T, Izu N, Kanematsu W. Is surface tension reduced by nanobubbles (ultrafine bubbles) generated by cavitation? Ultrason Sonochem 2019;52:13–8.
[32] Nazari S, Shafaei SZ, Gharabaghi M, Ahmadi R, Shahbazi B, Fan M. Effects of nanobubble and hydrodynamic parameters on coarse quartz flotation. Int J Min Sci Technol 2019;29(2):289–95.
[33] Zhang Z, Ren L, Zhang Y. Role of nanobubbles in the flotation of fine rutile particles. Miner Eng 2021;172:107140.
[34] Calgaroto S, Azevedo A, Rubio J. Flotation of quartz particles assisted by nanobubbles. Int J Miner Process 2015;137:64–70.
[35] Zhou W, Niu J, Xiao W, Ou L. Adsorption of bulk nanobubbles on the chemically surface-modified muscovite minerals. Ultrason Sonochem 2019;51:31–9.
[36] Ma F, Tao D, Tao Y. Effects of nanobubbles in column flotation of Chinese sub-bituminous coal. Int J Coal Preparat Utilizat 2019:1–17.
[37] Han H, Liu A, Wang H. Effect of hydrodynamic cavitation assistance on different stages of coal flotation. Minerals 2020;10(3):221.
[38] Oliveira H, Azevedo A, Rubio J. Nanobubbles generation in a high-rate hydrodynamic cavitation tube. Miner Eng 2018;116:32–4.
[39] Li C, Xing Y, Zhen K, Zhang H. Effect of dissolved air on the flotation behaviour of coal-kaolinite binary mixtures. Int J Coal Preparat Utilizat 2021;41(6):451–61.
[40] Lei W, Zhang M, Zhang Z, Zhan N, Fan R. Effect of bulk nanobubbles on the entrainment of kaolinite particles in flotation. Powder Technol 2020;362:84–9.
[41] Zhou S, Wang X, Bu X, Wang M, An B, Shao H, et al. A novel flotation technique combining carrier flotation and cavitation bubbles to enhance separation efficiency of ultra-fine particles. Ultrason Sonochem 2020;64:105005.
[42] Bu X, Zhang T, Chen Y, Peng Y, Xie G, Wu E. Comparison of mechanical flotation cell and cyclonic microbubble flotation column in terms of separation performance for fine graphite. Physicochem Probl Miner Process 2018;54:732–40.
[43] Ma F, Tao D, Tao Y, Liu S. An innovative flake graphite upgrading process based on HPGR, stirred grinding mill, and nanobubble column flotation. Int J Min Sci Technol 2021;31(6):1063–74.
[44] Zhang G, He, Wang H, Feng Y, Xie W, Zhu X. Application of mechanical crushing combined with pyrolysis-enhanced flotation technology to recover graphite and LiCoO2 from spent lithium-ion batteries. J Clean Prod 2019;231:1418–27.
[45] He Y, Zhang T, Wang F, Zhang G, Zhang W, Wang J. Recovery of LiCoO2 and graphite from spent lithium-ion batteries by Fenton reagent-assisted flotation. J Clean Prod 2017;143:319–25.
[46] Liu J, Wang H, Hu T, Bai X, Wang S, Xie W, et al. Recovery of LiCoO2 and graphite from spent lithium-ion batteries by cryogenic grinding and froth flotation. Miner Eng 2020;148:106223.
[47] Vanderbruggen A, Sygusch J, Rudolph M, Serna-Guerrero R. A contribution to understanding the flotation behavior of lithium metal oxides and spheroidized graphite for lithium-ion battery recycling. Colloids Surf A Physicochem Eng Asp 2021;626:127111.
[48] Cheng Q, Marchetti B, Chen X, Xu S, Zhou X-D. Separation, purification, regeneration and utilization of graphite recovered from spent lithium-ion batteries - a review. J Environ Chem Eng 2022;10(2):107312.
[49] Peng W, Qiu Y, Zhang L, Guan J, Song S. Increasing the fine flaky graphite recovery in flotation via a combined Multiple Treatments technique of middlings. Minerals 2017;7(11):208.
[50] Öney Ö, Samanli S. Determination of optimal flotation conditions of low-grade graphite ore. E3S Web Conf. 2016;8:01002.
[51] Kaya O, Canbazoglu M. A study on the floatability of graphite ore from yozgat Akdağmadeni (Turkey). J Ore Dress 2007.
[52] Yang X, Bu X, Xie G, Chelgani, SC. A comparative study on the influence of mono, di, and trivalent cations on the chalcopyrite and pyrite flotation. J Mater Res Technol 2021;11:1112–22.
[53] Bu X, Xie G, Peng Y, Chen Y. Kinetic modeling and optimization of flotation process in a cyclonic microbubble flotation column using composite central design methodology. Int J Miner Process 2016;157:175–83.
[54] Bu X, Xie G, Peng Y, Ge L, Ni C. Kinetics of flotation. Order of process, rate constant distribution and ultimate recovery. Physicochem Probl Miner Process 2017;53(1):342–65.
[55] Gharai M, Venugopal R. Modeling of flotation process-an overview of different approaches. Miner Process Extract Metall Rev 2015;37.
[56] Vaziri Hassas B, Guven O, Hassanzadeh A. An investigation of the recovery and kinetics during the flotation of residual petroleum coke in lime calcination exhaust tailings. Int J Coal Preparat Utilizat 2021;41(9):617–27.
[57] Hassas BV, Kouachi S, Eskanlou A, Bouhenguel M, Çelik MS, Miller JD. The significance of positive and negative inertial forces in Particle-Bubble interaction and their role in the general flotation kinetics model. Miner Eng 2021;170:107006.
[58] Kouachi S, Hassas BV, Hassanzadeh A, Çelik MS, Bouhenguel M. Effect of negative inertial forces on bubble-particle collision via implementation of Schulze collision efficiency in general flotation rate constant equation. Colloids Surf A Physicochem Eng Asp 2017;517:72–83.
[59] Moradi B, Botte GG. Recycling of graphite anodes for the next generation of lithium ion batteries. J Appl Electrochem 2016;46(2):123–48.
[60] Weng S. Fourier transform infrared spectroscopy. 2nd ed. Beijing: Chemical Industry Press; 2010.
[61] Bu X, Xie G, Chen Y, Ni C. The order of kinetic models in coal fines flotation. Int J Coal Preparat Utilizat 2017;37:113–23.
[62] Crawford R, Ralston J. The influence of particle size and contact angle in mineral flotation. Int J Miner Process 1988;23(1):1–24.
[63] Wu Y-S, Wang Y-H, Lee Y-H. Performance enhancement of spherical natural graphite by phenol resin in lithium ion batteries. J Alloys Compd 2006;426(1):218–22.
[64] Çilek EC, Yılmazer BZ. Effects of hydrodynamic parameters on entrainment and flotation performance. Miner Eng 2003;16(8):745–56.
[65] Dai Z, Fornasiero D, Ralston J. Particle–bubble collision models — a review. Adv Colloid Interface Sci 2000;85(2):231–56.

[66] Gupta A, Yan D. Mineral processing design and operations. 2nd ed. Amsterdam: Elsevier; 2016. p. 689–741 *[Chapter 18] - Flotation)*.
[67] Shahbazi B, Koleini SMJ. Effect of dimensionless hydrodynamic parameters on coarse particles flotation. Asian J Chem 2008;20:2180–8.
[68] Li H, Afacan A, Liu Q, Xu Z. Study interactions between fine particles and micron size bubbles generated by hydrodynamic cavitation. Miner Eng 2015;84:106–15.
[69] Zhang X, Wang Q, Wu Z, Tao D. An experimental study on size distribution and zeta potential of bulk cavitation nanobubbles. Int. J. Miner. Metall. Mater. 2020;27(2):152.
[70] Nazari S, Shafaei SZ, Gharabaghi M, Ahmadi R, Shahbazi B, Tehranchi A. New approach to quartz coarse particles flotation using nanobubbles, with emphasis on the bubble size distribution. Int J Nanosci 2018;19(1):1850048.
[71] Soga Y, Imanaka H, Imamura K, Ishida N. Effect of surface hydrophobicity on short-range hydrophobic attraction between silanated silica surfaces. Adv Powder Technol 2015;26(6):1729–33.
[72] Zhou W, Ou L, Shi Q, Feng Q, Chen, H.. Different flotation performance of ultrafine scheelite under two hydrodynamic cavitation modes. Minerals 2018;8(7):264.
[73] Gu G, Sanders RS, Nandakumar K, Xu Z, Masliyah JH. A novel experimental technique to study single bubble–bitumen attachment in flotation. Int J Miner Process 2004;74(1):15–29.
[74] Chipakwe V, Jolsterå R, Chelgani SC. Nanobubble-assisted flotation of apatite tailings: insights on beneficiation options. ACS Omega 2021;6(21):13888–94.
[75] Fan M, Tao D, Honaker R, Luo Z. Nanobubble generation and its applications in froth flotation (part III): specially designed laboratory scale column flotation of phosphate. Min Sci Technol 2010;20(3):317–38.
[76] Oliveira JF, Saraiva SM, Pimenta JS, Oliveira APA. Kinetics of pyrochlore flotation from Araxá mineral deposits. Miner Eng 2001;14(1):99–105.
[77] Chen Y, Chelgani SC, Bu X, Xie G. Effect of the ultrasonic standing wave frequency on the attractive mineralization for fine coal particle flotation. Ultrason Sonochem 2021;77:105682.
[78] Alheshibri M, Craig VSJ. Differentiating between nanoparticles and nanobubbles by evaluation of the compressibility and density of nanoparticles. J Phys Chem C 2018;122(38):21998–2007.
[79] Thi Phan KK, Truong T, Wang Y, Bhandari B. Nanobubbles: fundamental characteristics and applications in food processing. Trends Food Sci Technol 2020;95:118–30.
[80] Vaziri Hassas B, Miller JD. The effect of carbon dioxide and nitrogen on pyrite surface properties and flotation response. Miner Eng 2019;144:106048.
[81] Brenner MP, Lohse D. Dynamic equilibrium mechanism for surface nanobubble stabilization. Phys Rev Lett 2008;101(21):214505.
[82] Zhang XH, Quinn A, Ducker WA. Nanobubbles at the interface between water and a hydrophobic solid. Langmuir 2008;24(9):4756–64.
[83] Hassas BV, Jin J, Dang LX, Wang X, Miller JD. Attachment, coalescence, and spreading of carbon dioxide nanobubbles at pyrite surfaces. Langmuir 2018;34(47):14317–27.
[84] Tao D. Role of bubble size in flotation of coarse and fine particles—a review. Separ Sci Technol 2005;39(4):741–60.
[85] Albijanic B, Ozdemir O, Nguyen AV, Bradshaw D. A review of induction and attachment times of wetting thin films between air bubbles and particles and its relevance in the separation of particles by flotation. Adv Colloid Interface Sci 2010;159(1):1–21.